Blue Stragglers from Primordial Binary Evolution

Emilie Desrochers Karlsson

Lund Observatory
Lund University

2022-EXA189

Degree project of 15 higher education credits
June 2022

Supervisor: Ross Church

Lund Observatory
Box 43
SE-221 00 Lund
Sweden

Contents

1 List of Acronyms **2**

2 Popular science description **3**
2.1 Blue stragglers from mass transfer in binary star systems 3

3 Abstract **4**

4 Introduction **5**

5 Theory **7**
5.1 Luminosity and lifetime of main sequence stars 7
5.2 Metallicity and lifetime of main sequence stars 8
5.3 Tidal interactions, Roche lobe and mass transfer 8
5.4 Stability of mass transfer 10
5.5 Blue stragglers from primordial binary evolution 12
5.5.1 Case A: MS mass transfer 12
5.5.2 Case B: RGB mass transfer and common envelope evolution 12
5.5.3 Case C: AGB mass transfer 13
5.5.4 Mass transfer from stellar winds 13

6 Binary Star Evolution (BSE) **14**

7 Reproducing individual blue stragglers **14**
7.1 Method 15
7.2 Results 16
7.2.1 Close binaries ($a_0 \sim (10^0 - 10^1)R_\odot$) 16
7.2.2 Wide binaries ($a_0 \sim 10^3 R_\odot$) 17
7.3 Analysis 18
7.3.1 Close binaries ($a_0 \sim (10^0 - 10^1)R_\odot$) 18
7.3.2 Wide binaries ($a_0 \sim 10^3 R_\odot$) 21

8 Blue straggler populations from binary evolution **21**
8.1 Initial binary parameters 22
8.2 Method 22
8.2.1 Comparison with M67 23
8.3 Results 25
8.4 Analysis 27

9 Summary **29**

1 List of Acronyms

Acronym	Meaning
AGB	Asymptotic giant branch
BS	Blue straggler
HRD	Hertzsprung–Russell diagram
HG	Hertzsprung gap
IMF	Initial mass function
MS	Main sequence
PBE	Primordial binary evolution
RGB	Red giant branch
RLOF	Roche lobe overflow
TO	Turnoff
WD	White dwarf

2 Popular science description

2.1 Blue stragglers from mass transfer in binary star systems

Something that can significantly affect a person is its environment, and interactions with other people may change a person's trajectory of life permanently. The same is true for stars. The sun, for example, exists in a place within our galaxy where it is relatively calm. Stars in our neighborhood are far apart from each other and interactions between stars here are rare. The situation is however quite different in globular stellar clusters: spherical collections of stars that are tightly bound by gravity and are present both in the outer and central parts of our galaxy (Camargo and Minniti, 2019). Here, the density of stars is higher and interactions between them are much more likely. These interactions may affect the evolution of the stars.

One way to study the effects of these interactions is by looking at blue stragglers. In short, a blue straggler is a star that appears younger than the rest of the stars in the stellar cluster within which they reside. Stars in stellar clusters are believed to have been form out of the same gas cloud, which results in them being born at approximately the same time, hence making the blue stragglers stick out from the rest. Blue stragglers can form by two routes: through stellar collisions or by mass transfer between stars in binary systems: systems with two stars that are gravitationally bound and orbit each other. If the stellar density is high, it becomes more probable that a third star interacts with the binary system which might break it up, thus reducing the possibly for a blue straggler to form. On the other hand, in these environment stellar collisions are more common, which might enhance the blue straggler production.

The aim of my project is to study blue stragglers formed by mass transfer in binary systems in isolation, i.e. where the system is not affected by its environment. I will measure how commonly they form and how long they live. The results can then be compared to the M67 stellar cluster, where a total of 28 blue stragglers have been observed (Hurley et al., 2005), to see whether the derived number of blue stragglers is in agreement with observations, or if it is necessary to include the effects of the cluster environment to match observations. Answering these questions would enable a better understanding of how cluster environments and mass transfer can alter stellar evolution.

3 Abstract

Blue stragglers were first discovered as hotter and more luminous than the turnoff in the globular cluster M3. Their presence is typically explained by the interplay between stellar collisions and mass transfer in binary systems. In this thesis, I study blue stragglers produced from primordial binary evolution. This is done by both reproducing individual blue stragglers, to examine the different formation channels in great detail, but also by reproducing blue straggler populations, using a binary population synthesis, to investigate whether the age and/or metallicity of the population have an impact on their relative frequency. Furthermore, the derived relative frequency is compared with observations of the blue stragglers in the open cluster M67. The results show that primordial binary evolution form blue stragglers at any time during its evolution, but at different rates. Their relative frequency peaks at around 3-5 Gyr and is generally higher at lower metallicities. Furthermore, I show that the initial semi major axis and eccentricity of the binary determine the formation channel of the blue straggler. Also, that the most massive and luminous blue stragglers originate from the coalescence of contact binaries or large-scale mass transfer in close binary systems. The derived relative frequency of blue stragglers from primordial binary evolution was however too low to agree with observations of M67, indicating that the cluster environment likely was partly responsible for shaping the blue straggler population.

4 Introduction

A blue straggler (BS) is a main sequence (MS) star that, based on its magnitude (luminosity) and colour (temperature), appears younger than the rest of the stars in the cluster it inhabits. Stars in stellar clusters are assumed to be born at approximately the same time, formed from a single molecular cloud. The clusters should therefore, at any time, have a well defined turnoff (TO) mass because of the inverse proportionality between stellar mass and MS lifetime. However, Sandage (1953) found a group of stars bluer (hotter) and more luminous than the TO mass in the globular cluster M3. This could be seen in a Hertzsprung–Russell diagram (HRD), in which all MS stars follow a roughly linear effective temperature-luminosity relationship on a logarithmic scale, with a "turn" at the top, corresponding to the TO point. The existence of these stars was surprising and not expected from the theory established about stellar evolution, since they should already have left the MS. Nevertheless, these stars, later named blue stragglers, are present in globular clusters, open clusters, the field (Boffin et al., 2015), in dwarf spheroidal galaxies (Mateo et al., 1991) (Zhao et al., 2012), and in the Milky Way bulge (Clarkson et al., 2011).

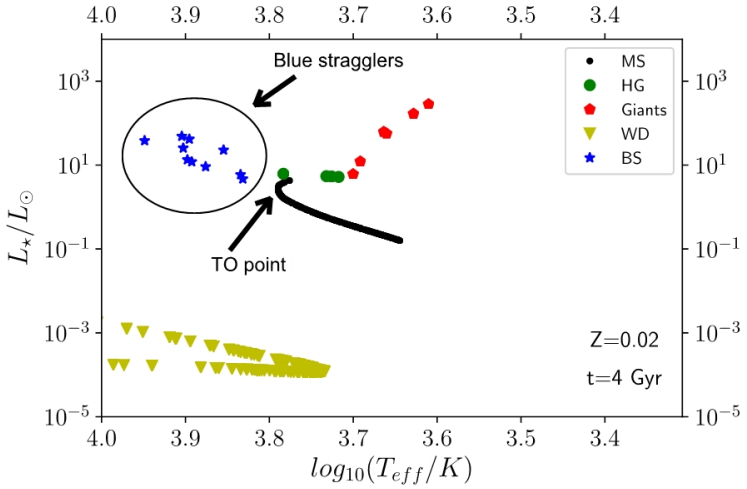

Figure 1: An illustration of where the blue stragglers and the turnoff point can be found in a Hertzsprung–Russell diagram.

BSs are believed to form by two different routes; by stellar collisions in dense environments such as in the cores of stellar clusters, and from mass transfer in binary star systems. In both cases, the star is rejuvenated by gaining hydrogen rich material, increasing the amount of fuel available for fusion, thus extending its lifetime.

While direct collisions between stars may be rare, even in dense clusters, close encounters can be enough to boost the BS formation rate. For example, nearby stars can in-

crease the eccentricity of a binary system, which may cause the two stars to merge and form a BS when they meet at periastron Hurley et al. (2005). Furthermore, interactions between a binary and a third star may harden the binary by transferring energy to the third star, which might increase the possibility of mass transfer Mateo et al. (1990). On the other hand, kinetic energy can also be transferred to the binary from the third star, potentially breaking up the binary system and thus preventing the BS formation. For these reasons, the presence of BSs in stellar clusters can be used to study dynamical effects arising from the environment of the cluster. Some work has been done, taking into account cluster dynamics, e.g. Hurley et al. (2005), Hurley et al. (2001), who showed that the cluster environment plays a significant role in shaping the BS population in the open cluster M67. However, complete N-body models for rich stellar clusters are numerically challenging and complicated. It would therefore be convenient to have a reference model of how often BSs form from the evolution of primordial binaries in isolation, unaffected by cluster dynamics, which is the primary question this paper will attempt to answer.

BSs found in the field are believed to form predominately by mass transfer in binary systems Preston and Sneden (2000). Observations of field BSs is therefore the most appropriate way to study the effect of mass transfer from PBE, that is unaffected by its environment. However, the lack of a well defined TO mass in these regions makes them difficult to identify. Luckily, it is possible to detect field BSs using other techniques. Jofré et al. (2016) studied the $\alpha-$rich stars located in the Galactic thick disc with masses exceeding 1.4 $M_{\odot}$. These stars were previously suggested to be young by e.g. Martig et al. (2015) and therefore typically called the "young $\alpha-$rich stars". However, Jofré et al. (2016) provided evidence showing that these stars may be a result of mass transfer in binary systems, potentially being evolved blue stragglers, thus not necessarily younger than the rest of the $\alpha-$rich population. For instance, they found that more of the "young" stars with masses above 1.4 $M_{\odot}$ were in binary systems compared to the "old" stars with masses below 1.2 $M_{\odot}$. Additionally, the "young" stars appeared to not follow the relationship between the [C/H] ratio and mass suggested by Lagarde et al. (2012) for single stars in isolation. By including mass transfer in binary evolution however, they were able to replicate the apparent [C/H] versus mass relationship for the "young" stars. Better understanding of the formation of blue stragglers and how to detect them can therefore provide more accurate estimations of the age of stellar populations, which further can be useful when studying the evolution of the Milky Way.

In this project, BSs formed from primordial binary evolution (PBE) have been studied in great detail. This has been done with the help of the rapid binary evolution synthesis code BSE by Hurley et al. (2002). In section 5, I first present some background theory on how the luminosity and metallicity affect MS lifetime, tidal interactions and mass transfer in binary systems and the different routes to form BSs from PBE. In section 6 the binary star evolution (BSE) synthesis code, used throughout the project, is described. The project was divided into two parts; I first reproduce individual BSs from

PBE to examine how the choice of initial binary parameters, such as initial semi major axis and masses of the two components determines the formation pathway of the BSs and their properties, e.g. the BS lifetime, mass and the ratio of BS mass to TO mass. The latter is of particular importance when doing real observations, in terms of their detectability. The reproduction of individual BSs from PBE is described in section 7. The second part, presented in section 8, involved the reproduction of BS populations from PBE and to study whether the age or metallicity of the evolved binaries affect their relative frequency. Here, the initial binary parameters were generated by probability distributions which are described in section 8.1. Similar initial binary parameters were assumed for all different metallicities, thus ignoring the anticorrelation between metallicity and close binaries fraction, suggested by e.g. Moe et al. (2019) and Wyse et al. (2020). In the end, I compare the derived frequency of BSs from PBE to the number of BSs observed in M67, to examine whether PBE alone is capable to explain all the BSs, or if cluster dynamics is needed to be included. Finally, in section 9, I summarize the project including the most important results and conclusions.

5 Theory

5.1 Luminosity and lifetime of main sequence stars

From the theory of stellar evolution Eldridge and Tout (2019) showed that the luminosity for zero-age solar-like stars on the MS with homologous structure is proportional to its mass by

$$L \propto M^{71/13} \approx M^{5.5} \tag{1}$$

From this equation it is clear that a small increase in mass leads to a large increase in luminosity, due to the power-law relationship. In other words, a massive star is much more luminous than a smaller one. Furthermore, there is a relationship between the MS lifetime (τ_{MS}) of a star and its luminosity. The MS lifetime of a star depends on how fast it burns its nuclear fuel. The amount of fuel available for fusion is proportional to the stellar mass while the luminosity determines how fast the fuel is consumed. For homologous solar-like stars, Eldridge and Tout (2019) state that the relation is given by

$$\tau_{MS} \propto \frac{M}{L} \propto M^{-4.5} \tag{2}$$

Hence, massive stars live much shorter lives than less massive stars.

One consequence of the relation given in equation 2 is that if a population of stars have the same age and composition, there exists, at any given time, a so-called turnoff mass (M_{TO}), for which all stars with mass $M < M_{TO}$ are still on the MS and all stars with $M > M_{TO}$ have already evolved to subsequent stellar phases. The value of the M_{TO} is a decreasing function of time, as illustrated in figure 1 in section 7.2.

5.2 Metallicity and lifetime of main sequence stars

In radiative regions inside stars, the luminosity can be expressed as

$$L(r) \propto \kappa^{-1} T^3 \frac{dT}{dr} \tag{3}$$

by rearranging the equation for the temperature gradient for radiative transfer Mowlavi et al. (1998). Here, T is the temperature and κ is the opacity. Hence, an increase in opacity leads to a decrease in luminosity. Decreasing the surface luminosity, (for a fixed mass), increases the MS lifetime, as shown in equation 2.

For solar-like stars, the main source of opacity in the surface regions is H^- bound-bound and H^- bound-free transitions, and the amount of H^--ions increases with metallicity, since the electrons from the ionized metals are needed to form H^- Gray (2008). Metal-rich solar-like stars therefore tend to stay on the MS longer than metal-poor ones.

5.3 Tidal interactions, Roche lobe and mass transfer

Before discussing how BSs can be formed by mass transfer between stars in binary systems, it is necessary to introduce the concept of Roche lobe and Roche lobe overflow (RLOF). If the stars in a binary system are close, so that their radii are of the same order of magnitude as their orbital separation, then tidal forces becomes strong. Tidal interaction might distort the shape of the stars and therefore, the gravitational potential will no longer simply be proportional to $1/r$. Consequently, quantities like the specific angular momentum $\mathbf{h} = \mathbf{r} \times \dot{\mathbf{r}}$ and the Laplace-Runge-Lenz vector $\mathbf{e}$, which has magnitude e equal to the orbital eccentricity, are no longer conserved. More, stable tidal equilibrium can be defined as the minimum in energy of the system for a given angular momentum. Eldridge and Tout (2019) showed that this is achieved when the orbit is circular and synchronized. The latter is obtained when the spin of the star is synchronized with the orbital angular velocity.

If the binary system has achieved circularisation and synchronization and the potential (Φ) is given by the sum of the gravitational potential and rotational kinetic energy $\Phi = \phi_G + \phi_\omega$, then one can show, using the Euler momentum equation

$$\frac{1}{\rho} \nabla P + \nabla \mathbf{\Phi} = 0 \tag{4}$$

where ρ and P are the density and pressure, respectively. Taking the curl of equation 4 gives

$$\nabla P \times \nabla \rho = \mathbf{0} \tag{5}$$

The relation given by equation 4 implies that the gradients of P and $\mathbf{\Phi}$ are parallel, meaning that a surface where the pressure is constant is also a surface where the potential

is constant. This will also be a surface where the density is constant, because of equation 5. Additionally, if the chemical composition is uniform, also the temperature will be constant on a surface of constant $\mathbf{\Phi}$. One can approximate this potential by the gravitational potential of two point masses at the positions of the centre of the two stars

$$\mathbf{\Phi} = \frac{-GM_1}{\sqrt{x^2+y^2+z^2}} + \frac{-GM_2}{\sqrt{(x-a)^2+y^2+z^2}} - \frac{1}{2}\frac{GM}{a^3}\left[\left(x - \frac{a}{1+q}\right)^2 + y^2\right] \tag{6}$$

with star 1 at origin with mass M_1 and star 2 at $(a, 0, 0)$ with mass M_2. q is the mass ratio $q = M_1/M_2$, G is the gravitational constant, M is the total mass and a is the semi major axis Eldridge and Tout (2019).

Potential surfaces which obey the relations described above are often referred as equipotentials. Material in stars fill up to an equipotential and will therefore take its shape. If the two stars are small compared to their separation, the equipotentials are spheres around the positions of the two stars. Far away from the binary system, the equipotentials are also spheres, but now around the whole system. The surface of interest when discussing mass transfer between stars in binary systems is the equipotential that surrounds both stars and intersect in a point between them. This point corresponds to the first (L_1) of the total five Lagrangian points that every two-body-system contain. Lagrangian points are stationary points where the gradient of the potential is zero. The equipotential surface that passes through L_1 represents the largest either of the stars can grow before material will become more gravitationally attracted to the other star. This surface is known as the Roche lobe.

When the size of one of the stars in the system exceeds its Roche lobe, material will start to flow towards the other star. This phenomenon is known as Roche lobe overflow (RLOF). If non of the stars fill their Roche lobe the system is categorized as a detached. If one of the stars fill it, the system is semi-detached. Finally, if both stars fill their Roche lobe at the same time, the two stars are touching at the L_1 point and the system is a contact binary.

The Roche lobe radius R_L is defined as the radius of the sphere enclosing the same volume as the Roche lobe and was fitted by Eggleton (1983) for star 1

$$\frac{R_L}{a} = \frac{0.49q^{2/3}}{0.6q^{2/3} + log_e\left(1+q^{1/3}\right)} \tag{7}$$

with an accuracy of better than 1% for $0 < q < \infty$. For analytic solutions, Paczyński (1971) provided a formula with accuracy better than 3% for $0 < q < 0.8$

$$\frac{R_L}{a} = 0.462\left(\frac{M_1}{M}\right)^{\frac{1}{3}} \tag{8}$$

The rate of which mass is transferred from star 1 to star 2 mainly depends on how much star 1 overfill its Roche lobe, but also on the density at L_1. For the sun, Eldridge and Tout (2019) state that the mass transfer rate can be approximated by

$$\dot{M}_1 \approx 6 \times 10^{-10} M_\odot yr^{-1} e^{25\Delta R/R_1} \tag{9}$$

where $\Delta R = R_1 - R_L$. For a red giant however, the mass transfer rate is well approximated by

$$\dot{M}_1 \approx -10 \frac{M_1}{M_\odot} \left(\frac{yr}{P}\right) \left(\frac{\Delta R}{R_1}\right)^3 M_\odot yr^{-1} \tag{10}$$

where P is the orbital period.

A final word on this topic is that tides typically are strong enough (at least for binaries that are close enough to allow for mass transfer) that circularisation and synchronization both are achieved before RLOF occurs Eldridge and Tout (2019).

5.4 Stability of mass transfer

When a star loses mass, both hydrostatic and thermal equilibrium is perturbed. The star will then try to adjust its size accordingly, to obtain a new equilibrium radius. In order to determine whether the mass transfer is stable or not, one often considers three derivatives of radii with respect to the mass of the mass-losing star, and compare them. To examine the stability I follow the approach of Eldridge and Tout (2019). From now, I will denote the evolved star (the initially more massive of the two) as the donor with mass M_d while the initially less massive star is the accretor with mass M_a.

The first derivative describes the response of the Roche lobe radius of the donor upon mass loss, when the total mass and angular momentum of the system is conserved

$$\zeta_L = \left(\frac{\partial log R_L}{\partial log M_d}\right)_{M,J} \tag{11}$$

which was approximated by Tout et al. (1997) as

$$\zeta_L \approx 2.13q - 1.67. \tag{12}$$

From equation 11 and 12 we see that the Roche lobe of the donor shrinks as a consequence of mass loss from the donor to the accretor if $q = \frac{M_d}{M_a} > 0.78$. If $q < 0.78$ the Roche lobe expands.

The first response of the donor is to regain hydrostatic equilibrium, which occurs on a dynamical timescale. Since the dynamical timescale is much shorter than the thermal timescale [1], this process can be approximated to be adiabatic. In this context, adiabatic

[1] The approximate time required for a star to radiate all its thermal energy if nuclear fusion in its core suddenly stopped.

means that the entropy in each layer of the star remains constant, i.e. the timescale is too short for adjacent layers to interchange energy Ivanova (2015). The second derivative therefore describes the response of the radius of the donor upon mass loss, at constant entropy s and composition X

$$\zeta_{ad} = \left(\frac{\partial log R_d}{\partial log M_d}\right)_{s,X} \tag{13}$$

The sign of ζ_{ad} turns out to depend on the properties of the envelope of the donor. If the envelope is radiative, i.e. if radiation is the main energy transport process, then $\zeta_{ad} > 0$. The stellar radius then shrinks as a response of mass loss. On the contrary, if the envelope is convective, so that the energy transport occurs mainly by convection, then $\zeta_{ad} < 0$ and the star expands upon mass loss.

The response of the radius on a thermal timescale, when the star has regained both hydrostatic and thermal equilibrium, is described by the third derivative

$$\zeta_{eq} = \left(\frac{\partial log R_d}{\partial log M_d}\right)_{X} \tag{14}$$

again with constant composition X. According to Eldridge and Tout (2019), $\zeta_{eq} > 0$ for MS stars and $\zeta_{eq} < 0$ for red giants and stars in the Hertzsprung gap (HG) [2].

The timescale of the mass transfer can be estimated by comparing the three derivatives. If $\zeta_L > \zeta_{ad} > 0$, i.e. the Roche lobe radius shrinks faster than the stellar radius, then the value of ΔR increases with time. Since the rate of the mass transfer is strongly dependent on ΔR, (see equation 9 and 10) this will lead to a runaway process and the mass transfer proceeds on a dynamical timescale $\tau_{dyn} \approx 10 - 100$ years. A similar situation will occur if the stellar radius expands faster than the Roche lobe radius. An example of a situation where the mass transfer is dynamically unstable is when a red giant fills its Roche lobe. If the accretor star is less massive, so that $q = \frac{M_d}{M_a} > 1$, then the Roche lobe shrinks upon mass loss. Red giants have convective envelopes so they expand as a response of mass loss. Thus, ΔR and therefore $\dot{M}$ increase over time and the mass transfer is unstable. Usually, the accretor can not accrete mass at such high rate and the transferred mass ends up in a common envelope around the two stars.

If $\zeta_{eq} < \zeta_L \leq \zeta_{ad}$, then the donor star will at first shrink faster than the Roche lobe, thus being dynamically stable. However, the star expands on a thermal timescale and the mass transfer also proceeds on a thermal timescale $\tau_{th} \approx 10^5 - 10^6$ years. This is typically the case when RLOF occurs for a star in the HG with radiative envelope.

Finally, if ζ_L is less than both ζ_{eq} and ζ_{ad}, then the donor will shrink faster than its Roche lobe on both a dynamical and thermal timescale and RLOF will not happen again un-

[2]Stars in the HG have terminated core hydrogen burning but have not yet entered the red giant branch.

less triggered by its own nuclear evolution, or if the system loses orbital angular momentum, causing the orbit to decay. The mass transfer will thus proceed either on a nuclear timescale $\tau_{nuc} \approx 10^7 - 10^9$ years, or on the timescale orbital angular momentum is taken away from the system.

From now on, mass transfer that occurs on a dynamical timescale will be considered unstable while mass transfer on thermal and nuclear timescales is stable.

5.5 Blue stragglers from primordial binary evolution

From previous subsections we have discussed what a BS is, how mass transfer occurs and how to examine its stability. We are now ready to explore the different routes to form BSs from PBE. I will first consider BSs formed as a consequence of mass transfer trough RLOF and then proceed with BSs formed by stellar wind accretion.

Mass transfer as a result of RLOF is usually divided into three different cases; A, B and C, each described separately below.

5.5.1 Case A: MS mass transfer

Case A is when RLOF and thus mass transfer occurs when the donor star is on the MS. This can happen for close binaries with separations on the order of a few solar radii. If the two stars are close enough, both stars might fill their Roche lobes, thus being in direct contact. RLOF can occur as a result of either evolution (the radius of MS stars increases with time) or because of loss of orbital angular momentum which would cause the orbital separation and thus the Roche lobe to decrease (see equation 8). The contact binary will eventually merge and if the resulting single star has a mass above the TO it will be a BS. If only the donor star fills its Roche lobe, the accretor might become a BS before the merger.

5.5.2 Case B: RGB mass transfer and common envelope evolution

Case B mass transfer is when the donor is on the red giant branch (RGB). During the giant phases, the stellar radius expands rapidly and can reach a size of up to about $200R_\odot$ for stars with initial masses below approximately $1.3 - 1.5M_\odot$. For stars with initial masses between $2 - 3M_\odot$ however, the radius only increases to about $30 - 100R_\odot$ Boffin (2015).

As previously described, RLOF on the RGB is typically unstable, since the giant expands as a result of mass loss while its Roche lobe shrinks if $q > 0.78$. Dynamically unstable mass transfer leads to common envelope evolution, where the degenerate core of the giant and the accretor star are in orbit inside the low-density envelope of the original giant. What follows from here is not well established, but some frictional process is

believed to cause the orbit of degenerate core and secondary star to decay Eldridge and Tout (2019). The amount of orbital energy lost as a result of the orbital decay is instead transferred to the envelope resulting in loss of material in winds. If the total orbital energy is larger than the binding energy of the envelope, the whole envelope can be lost while the core and accretor still are quite wide. On the contrary, if the orbital energy is less than the binding energy of the envelope, the core and secondary star will coalesce to a single star.

I should add that case B mass transfer can be stable providing that the conditions are right. It turns out to exist a critical value of the mass fraction $q_{crit} = M_d/M_a$, for which binaries with $q < q_{crit}$ have stable mass transfer while binaries with $q > q_{crit}$ have unstable mass transfer. The value of q_{crit} is debatable and depends on a lot of factors, e.g. if the mass transfer is conservative or not, the structure of the envelope of the giant and the core mass. One consequence of this is that if the donor star manages to lose enough mass by e.g. stellar winds before RLOF occurs, it can avoid common envelope evolution.

5.5.3 Case C: AGB mass transfer

If the donor star is on the asymptotic giant branch (AGB) the mass transfer is classified as case C. If the binary is wide enough it is possible that RLOF on the RGB is avoided and instead occurs on the AGB. During the AGB phase, the star undergoes a phenomenon normally called thermal pulses, a cyclic repeating process where a helium-burning shell ignites in a semi-explosive way, resulting in large amount of released energy, causing the star to expand and cool Beccari and Carraro (2015). During this phase, stars with initial masses above $3M_\odot$ can reach a size of $800R_\odot$ Boffin (2015).

A star loses mass through stellar winds during all phases of its evolution, but at different rates. When the star is on the AGB, in particular when undergoing thermal pulses, the mass loss through winds is of great importance, since the envelope during this phase is as expanded and cool as ever, and thus can easily be "ripped of" Beccari and Carraro (2015). It is therefore possible for a binary system, which has an initial mass ratio of $q > 1$ to reach a value of $q < q_{crit}$ before RLOF occurs (providing that the system is wide enough), and hence have stable mass transfer.

5.5.4 Mass transfer from stellar winds

As discussed above, a star loses mass not only by RLOF but also via stellar winds. Some material lost from one star in a binary could be accreted by the second star, potentially pushing the accretors mass above the TO, thus making it a BS. RLOF is therefore not a requirement in the formation of BSs from PBE.

Here, I will consider mass transfer from stellar winds for detached binaries, i.e. when non of the two stars fill their Roche lobes. To get a sense of the rate at which a star loses

mass through winds I first present some values of the mass loss rate at different stages of evolution. The sun loses $10^{-14} M_\odot$ yr^{-1} through winds, for red giants with luminosities between $50 - 200 L_\odot$ the value is about $10^{-10} - 10^{-8} M_\odot$ yr^{-1} while for AGB star the rate can reach a value of up to $10^{-4} M_\odot$ yr^{-1} Boffin (2015). The BS formation from wind accretion is hence of greatest importance for binary systems where the donor is on the AGB.

The mean accretion rate from the donor to the accretor, $\left\langle \dot{M}_a \right\rangle$, is typically estimated using the Bondi and Hoyle (1944) accretion rate,

$$\left\langle \dot{M}_a \right\rangle = \frac{-1}{\sqrt{1-e^2}} \left(\frac{GM_d}{v_W^2} \right)^2 \frac{\alpha_W}{2a^2} \frac{1}{(1+v^2)^{3/2}} \dot{M}_d \tag{15}$$

where $v^2 = \frac{v_{orb}^2}{v_W^2}$ and $v_{orb}^2 = \frac{G(M_d+M_a)}{a}$. $\dot{M}_d$, v_{orb}, v_M, e are the rate at which the donor star loses mass, the orbital velocity, the wind velocity and eccentricity, respectively. α is an efficiency parameter of the order of ~ 1.

6 Binary Star Evolution (BSE)

For this project, the BSE (binary star evolution) code by Hurley et al. (2002) was used. As the name reveals, this is a binary evolution algorithm, written in FORTRAN. It incorporates the single star evolution (SSE) model by Hurley et al. (2000) but it additionally includes necessary features of interacting stars in binary systems, such as mass transfer/accretion by both RLOF and stellar winds, common envelope evolution, merger, angular momentum loss mechanisms, as well as circularization and synchronization.

The inputs of BSE are the initial masses of the two zero-aged MS stars, their initial periods, eccentricity, metallicity and the maximum time to evolve the binary. The output includes data points in time for which the timestep-size can be specified in the input. At each timestep, BSE prints parameters such as the luminosities of the two stars, their radii, masses and the types of the two stars, which are the most important parameters when studying blue stragglers. The stellar types, (MS, RGB, AGB, white dwarf etc), corresponds to stellar evolutionary stages assigned by the SSE algorithm. More details about BSE can be found in the paper by Hurley et al. (2002).

7 Reproducing individual blue stragglers from binary evolution

As mentioned in the introduction, my project consist of two parts. In the first part, which I present here, I reproduce individual BSs and analyze how the choice of initial binary parameters affects the outcome for the BSs. In particular, I examined how the

choice of initial semi major axis and initial masses determined the formation pathway for the BSs, the stability of mass transfer, the BS lifetime, the maximum BS mass and the maximum ratio between the BS mass and TO mass.

Understanding what initial binary parameters are important when considering the BS formation could potentially be necessary when interpreting the frequencies of BSs, found from either observations or simulations in different regions such as globular or open clusters, with different properties, such as age or metallicities. The ratio between the BS mass and TO mass ($\frac{M_{BS}}{M_{TO}}$) is of particular importance when doing real observations, since BSs with $\frac{M_{BS}}{M_{TO}}$-values close to one will be hard to detect. This is because they would have almost the same luminosity as a MS star with mass equal to the TO, thus not be so prominent in a HRD and could therefore easily be missed.

7.1 Method

Here, I present the method used to obtain the results presented in the next subsection. All analysis was performed using BSE along with self written code in Python.

In order to identify BSs I first need a function which calculates the TO mass at any metallicity and at any given time during the binary evolution. This was done by running BSE for 100 single stars with masses between (0.8-10)$M_\odot$. The reason why doing this for single stars was to avoid any binary complexity. The lower limit was chosen since stars with lower masses, even if they were born at the very beginning of the Universe, will still be on the MS today. Stars with masses above $10M_\odot$ have lifetimes too short to be of any importance for BSs. The MS lifetimes for the 100 stars were extracted from BSE. The function which calculates the TO mass at any given time and metallicity, $M_{TO}(t, Z)$, was obtained using Scipy's module interp1d which uses interpolation to fit a function to data points.

I began by analyzing how the choice of initial semi major axis, a_0, and initial mass of the donor affect the time at which a BS is formed and its lifetime. This was done for three binaries, where the initial mass of the accretor was kept constant at $M_a = 1M_\odot$ while the initial donor mass was changed between $M_d = (1.5, 2.0, 2.5)M_\odot$. The initial eccentricity e_0 and the metallicity Z were set to 0.5 and 0.02, respectively. For the three binaries, the time at which a BS was formed, t^{BS}_{BEG}, as well as when it ends to be a BS, t^{BS}_{END}, were plotted versus a_0, as shown in figure 3 and 7. t^{BS}_{BEG} was defined to be the time, t, in BSE for when either of the two stars, providing it was still a MS star, had a mass of $M > 1.01M_{TO}(t)$. A small tolerance was chosen to avoid any uncertainties in the interpolation. Furthermore, t^{BS}_{END} was defined as the time when the BS left the MS and began the subgiant-phase in the HG. Additionally, the BS lifetime, i.e. $t^{BS}_{END} - t^{BS}_{BEG}$, was plotted for the three binaries, versus a_0, and is presented in figure 4 and 8. For further analysis, also the maximum BS mass versus a_0, was plotted for the three binaries in figure 5 and 9. To examine the detectability of the BSs, as in how prominent they would

be in a HRD, the maximum value of the ratio M_{BS}/M_{TO} was plotted versus a_0. These results are shown in figure 6 and 10.

7.2 Results

Both close ($a_0 \sim 10^1 R_\odot$) and wide ($a_0 \sim 10^3 R_\odot$) binaries formed BSs. The process which resulted in the formation of the BS depended on the value of a_0. Furthermore, it turned out to exist a region of values of a_0 where only unstable mass transfer occurred, where $q > q_{crit}$ thus leading to common envelope evolution, preventing any BS formation. The results and analysis were therefore divided into two parts, corresponding to two regions where stable mass transfer occurred. The result are first presented for close binaries with $a_0 \sim (10^0 - 10^1)R_\odot$, followed by wide binaries with $a_0 \sim 10^3 R_\odot$. Note that in figure 3-10 the data points are the results that should be considered. The lines between data points were added to obtain a clearer view.

In figure 2, the TO mass versus time is plotted for $Z = 0.02$ as well as the interpolated function, corresponding to $M_{TO}(t, Z = 0.02)$.

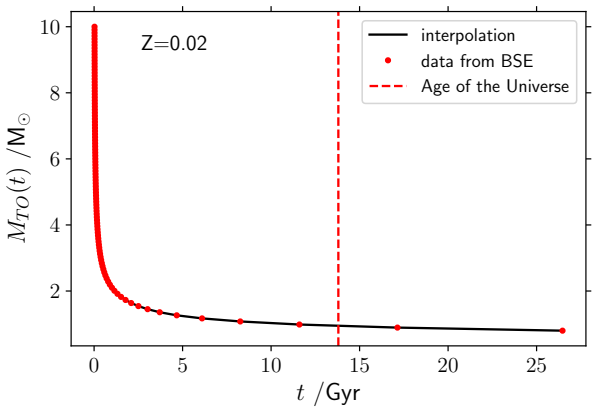

Figure 2: The turnoff mass versus time from BSE (red dots) and $M_{TO}(t, Z = 0.02)$ (black line). The red dashed line represents the age of the Universe.

7.2.1 Close binaries ($a_0 \sim (10^0 - 10^1)R_\odot$)

Figure 3 shows the time at which the system forms a BS, t^{BS}_{BEG}, and the time when it ends to be a BS, t^{BS}_{END}, as a function of initial semi major axis. The corresponding BS lifetimes are plotted in figure 4 whereas figure 5 shows the maximum BS mass. Finally, in figure 6 the maximum value of the ratio between the BS mass and the TO mass during its lifetime is plotted as a function of a_0.

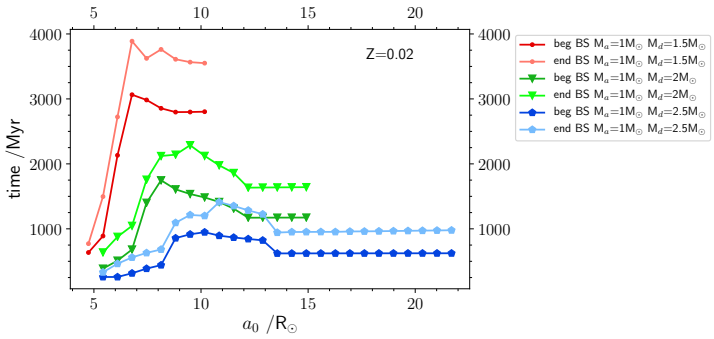

Figure 3: t^{BS}_{BEG} and t^{BS}_{BEG} versus initial semi major axis a_0 for close binaries.

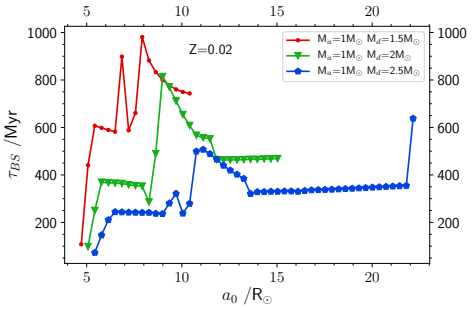

Figure 4: Blue straggler lifetime versus initial semi major axis a_0 for close binaries.

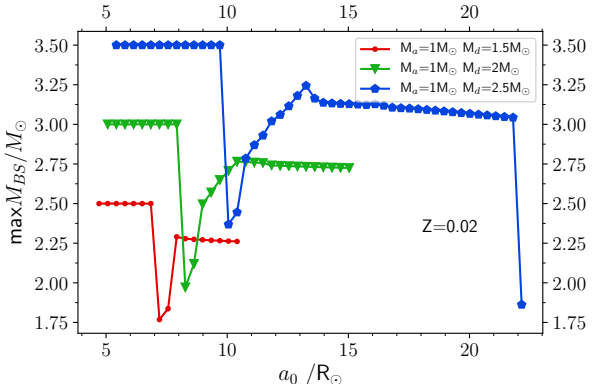

Figure 5: The maximum BS mass versus initial semi major axis a_0 for close binaries.

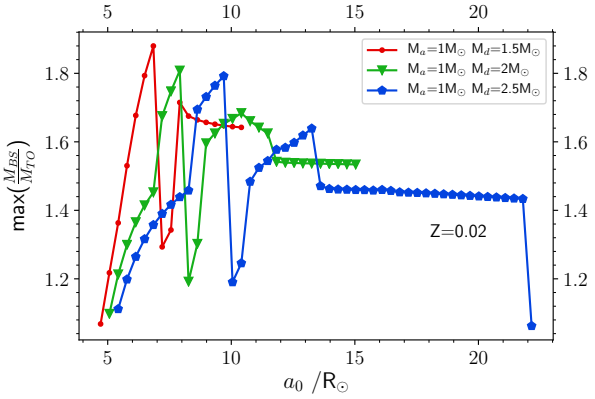

Figure 6: The maximum ratio between BS mass and TO mass versus initial semi major axis a_0 for close binaries.

7.2.2 Wide binaries ($a_0 \sim 10^3 R_\odot$)

Figure 7-10 show the corresponding four plots for the wider binaries.

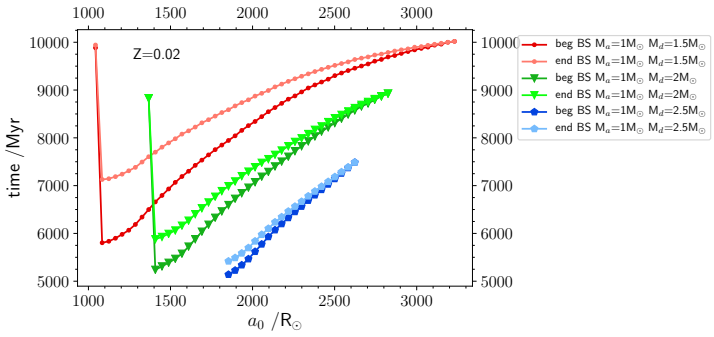

Figure 7: t^{BS}_{BEG} and t^{BS}_{BEG} versus initial semi major axis a_0 for wide binaries.

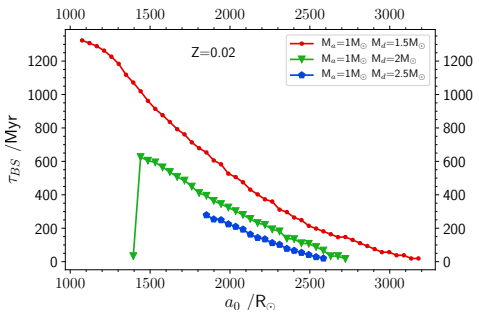

Figure 8: Blue straggler lifetime versus initial semi major axis a_0 for wide binaries.

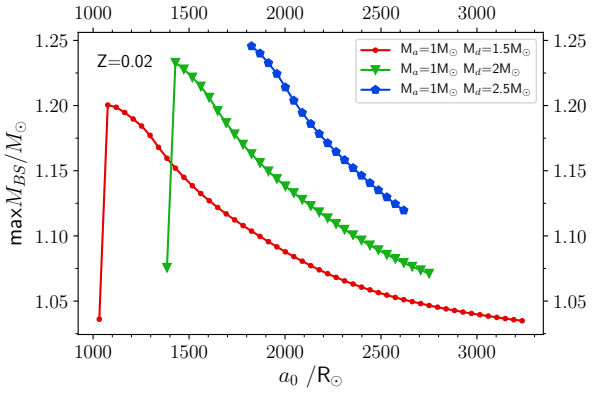

Figure 9: The maximum BS mass versus initial semi major axis a_0 for wide binaries.

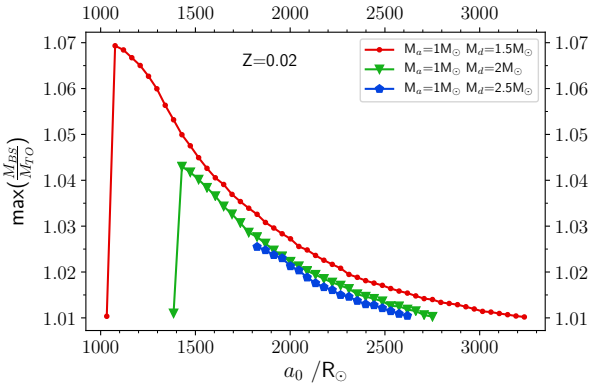

Figure 10: The maximum ratio between BS mass and TO mass versus initial semi major axis a_0 for wide binaries.

7.3 Analysis

Similarly in this subsection, I begin discussing the results for the close binaries, followed by the wider ones.

7.3.1 Close binaries ($a_0 \sim (10^0 - 10^1)R_\odot$)

In figure 3, there are three different processes leading to the formation of a BS. This could be read from the output of BSE which prints the type of the two stars (i.e. MS, HG, RGB etc.) when RLOF occurs and when a BS is formed. For the closest binaries, both stars fill their Roche lobes, thus being in direct contact. Eventually they merge and the resulting single star becomes a BS once its mass is above the TO. For a slightly larger initial semi major axis, the donor fills its Roche lobe on the MS and a BS is formed

when the donor is on the end of the MS or in the HG. The third process in figure 3, RLOF occurs when the donor star is already in the HG.

Still considering figure 3, there is an initial increase in t_{BEG}^{BS} as a function of a_0. This can be understood from equation 7; the Roche lobe radius increases as a increases. Consequently, the stars must evolve more for larger a_0 in order for RLOF to occur. Above some value of a_0 however, there is a decrease in t_{BEG}^{BS} as a function of a_0, ($a_0 \approx 7R_\odot$ for $M_d = 1.5M_\odot$, $a_0 \approx 8R_\odot$ for $M_d = 2M_\odot$ and $a_0 \approx 10R_\odot$ for $M_d = 2.5M_\odot$). Since increasing a_0 will make RLOF occur later, the donor will spend more time with its initial mass conserved. Therefore, increasing a_0 will lead to the donor leaving the MS earlier, thus the accretor will become a BS faster. The reason why we do not see this effect for closer binaries is because they form BSs before the donor leaves the MS.

For the third process, as already mentioned, RLOF occurs when the donor is in the HG. This corresponds to the region in figure 3 where t_{BEG}^{BS} and t_{END}^{BS} is roughly constant as a function of a_0, ($a_0 \sim (13.5 - 22)R_\odot$ for $M_d = 2.5M_\odot$). This might be explained by the fact that stars stay in the HG for very short periods comparing to their MS lifetime, $\tau_{HG} \ll \tau_{MS}$.

Now comparing the three different binary systems, we see that as the donor mass increases we get BSs for larger a_0. This is simply because the donor star gets larger thus all processes are shifted to larger values of a_0. Since the donor star is the one driving the mass transfer, t_{BEG}^{BS} decreases as its mass increases since more massive stars evolve faster.

The reason why we do not get any BSs for smaller separations is because they merge too fast for the resulting single MS star to ever have a mass above the TO mass during its lifetime. The merger will therefore just produce a more massive MS star which leaves the MS before the TO has fallen below the stellar mass. For wider systems however, RLOF will start when the donor star is on the RGB and will thus have dynamically unstable mass transfer since $q > q_{crit}$. This results in a common envelope evolution which typically prevents the BS formation. This explains the lack of BSs after some critical value of a_0, which is dependent on the two stellar masses.

In figure 4 the BS lifetime is plotted as a function of initial semi major axis. First, the lifetime increases as a function of a_0. This is because the merger occurs later for larger a_0 so the accretor will spend more time with its initial mass, thus increasing its lifetime. Here, the resulting single star does not become a BS directly after the merger but once its mass is above the TO. Then, the lifetime stays roughly constant ($a_0 \sim (5 - 6)R_\odot$ for $M_d = 1.5M_\odot$, $a_0 \sim (6 - 8)R_\odot$ for $M_d = 2M_\odot$ and $a_0 \sim (6.5 - 9)R_\odot$ for $M_d = 2.5M_\odot$). These are also merging systems but in contrast to the closer systems, the BS is formed immediately after the merger and since the BS mass is constant in this region (see figure 5), also the BS lifetime is constant. The BS lifetime for the second process, where

the donor star fills its Roche lobe on the MS and a BS is formed before the merger of the two stars, is complex and can not be explained only using the BS mass. Looking at the blue straggler lifetime for $M_a = 1M_\odot$ and $M_d = 1.5M_\odot$ (red dots in figure 4) there is a transition at around $a_0 = 7R_\odot$. There is a similar behaviour for the other binaries as well but for larger a_0. The odd behaviour of the lifetime in this region is because the merger occurs once the donor has left the main sequence and BSE assumes this will proceed like a common envelope evolution. Also, for some cases in this region, the mass ends up in the evolved star and the BS phase is therefore terminated since the donor is no longer a MS star. The peak of each curve corresponds to the smallest value of a_0 for which contact occurs after the BS phase is terminated. The BS lifetime is therefore not perturbed by common envelope evolution. The lifetime then again decreases, since more mass is transferred (see figure 5) and finally stays roughly constant as the BS mass is constant. The BS lifetime decreases as M_d increases. This can also be understood using the results in figure 5. More massive donor stars produce more massive BSs thus reducing their lifetimes.

The minimum of the BS mass in figure 5 corresponds to the smallest value of a_0 for which contact occurs after the donor has left the MS. Since BSE assumes that this proceeds like common envelope evolution (so that the BS phase is terminated) the maximum BS mass is the mass it has right before contact. The maximum BS mass then increases with a_0 because a larger fraction of the mass transfer occurs when the donor is in the HG where the stellar radius increases more rapidly, compared to when it is on the MS. The donor will therefore fill its Roche lobe by a larger amount and the rate of the mass transfer is therefore higher, producing more massive BSs.

In figure 6 the maximum of the ratio between the BS mass and the TO mass at that time is plotted as a function of a_0 for the three binary systems. The higher this ratio, the easier it will be to detect the BS since it will deviate more from the TO point in a HRD. The results show a similar behaviour when increasing M_d but shifted to the right for higher M_d-masses. However, for systems where RLOF occurs in the HG , (which is in the region where $\max\frac{M_{BS}}{M_{TO}}$ is constant as a function of a_0), there is a clear decrease for more massive donor stars. Increasing M_d decreases t_{BEG}^{BS} so there will be less effect on the overall evolution compared to making a massive star at $t = 0$. Another way to think about it is that M_{TO} is rapidly decreasing as a function of time, at least in the beginning of the evolution, since there is an inverse power law relationship between TO mass and time (as illustrated in figure 2). If t_{BEG}^{BS} happens sightly earlier in one case than another, the turnoff mass at that time will be much higher. This results in a lower value of $\max\frac{M_{BS}}{M_{TO}}$, even though M_{BS} gets larger for larger M_d.

7.3.2 Wide binaries ($a_0 \sim 10^3 R_\odot$)

The following will consider wide binaries forming BSs. Wide binaries produces BSs by two different processes: RLOF when the donor is on the AGB and by wind accretion. Mass transfer between the stars is stable once the donor star has lost enough mass so $q = \frac{M_d}{M_a} < q_{crit}$.

The results in figure 7 show that increasing M_d while keeping M_a constant produces BSs only at larger separations. For larger donor masses and smaller a_0, RLOF will happen before $q < q_{crit}$, thus being unstable. Less massive donor stars will not have to lose as much mass to achieve $q < q_{crit}$ and can thus have stable mass transfer for smaller values of a_0.

Also, increasing M_d decreases the range of semi major axes where BSs are formed. This is because increasing M_d decreases t^{BS}_{BEG}, so the TO mass at the time when the binary with $M_d = 2.5M_\odot$ form a BS will be much higher compared to at the time when a binary with $M_d = 1.5M_\odot$ form one, for a fixed value of M_a and a_0. This means that more mass is required to be transferred to the accretor star to push it beyond the turnoff mass if the mass transfer happen early in the evolution compared to later. This is justified by the results in figure 10, as M_d increases, $\max(\frac{M_{BS}}{M_{TO}})$ decreases to 1 for smaller values of a_0, even if the BS mass is higher, as shown in figure 9.

Finally, comparing the results for close and wide binaries we can conclude that close binaries form more massive BSs. The quantity M_{BS}/M_{TO} is much larger for close binaries, which makes them easier to detect. On the contrary, the lifetime τ_{BS} is roughly the same for close and wide binaries. An explanation for this is that t^{BS}_{BEG} is lower for close binaries and that $M_{TO}(t)$ decreases faster early in the evolution. The reason why t^{BS}_{BEG} is lower for close binaries is simply because they form BSs when the donor is either a MS star or in the HG while wide binaries form BSs when the donor is on the AGB, thus more evolved.

8 Blue straggler populations from binary evolution

The second part of the project involved estimating how often BSs are formed from PBE and whether the age and/or metallicity matters for their frequency. I also examine the initial conditions, such as the initial accretor mass and period, of the binaries making BSs. Finally, I compare the derived frequency of BSs from PBE to observations of BSs in the well studied open cluster M67. I also provide an example of a HRD, including 28 blue stragglers, corresponding to the number observed in M67 (Hurley et al., 2005).

8.1 Initial binary parameters

In section 7, only individual BSs were reproduced, with fixed initial binary parameters. To estimate their frequency and study BS populations however, the initial binary parameters need to be generated from a more realistic model, which is described in this subsection.

The probability distribution of donor masses were obtained according to the initial mass function (IMF), suggested by Kroupa (2001), for donor stars with masses between $(0.5 - 100)M_{\odot}$. The probability distribution of mass ratio $x = \frac{M_a}{M_d}$ was assumed to be constant with $x \in [0 : 1]$ (Moe and Di Stefano, 2017). Similarly, all initial eccentricities were assumed to be equally probable (Raghavan et al., 2010). A Gaussian probability distribution was used to generate the initial periods, peaking at $logP = 5.03$ with standard deviation of $\sigma_{logP} = 2.28$ where P is in days (Raghavan et al., 2010).

8.2 Method

To determine the frequency of BSs and its dependence on age and metallicity, 200 000 binaries were evolved using BSE, with initial binary parameters according to the ones described in subsection 8.1, for $t = (1, 3, 5, 8, 12)$ Gyr and metallicities $Z = (0.02, 0.01, 0.001)$. As in section 7, a BS was formed once either of the two stars had a mass of $M > 1.01M_{TO}(t, Z)$ while still being a MS star. The fraction of total number of BSs, as well as the fraction of BSs originating from close/wide binaries to the total number of evolved binaries, were plotted for the three different metallicites, versus time. Here, close/wide binaries were defined using the initial distance at periastron (given by $a_0(1 - e_0)$), instead of a_0 as in section 7. The BSs formed by binaries with inital periastron distance $a_0(1 - e_0) < 40R_{\odot}$ were defined as close, otherwise wide. For the BSs at $t = (1, 5, 12)$ Gyr and $Z = 0.02$, also $a_0(1 - e_0)$ was plotted versus the initial mass of the accretor.

For $Z = 0.02$ at $t = 4$ Gyr, 28 BSs as well as 800 single stars were plotted in a HRD, i.e. their luminosity versus effective temperature T_{eff}. The luminosities were generated by BSE while the effective temperatures were calculated using the Stefan–Boltzmann law:

$$T_{eff} = \left(\frac{L}{4\pi R^2 \sigma_{SB}} \right)^{\frac{1}{4}} \tag{16}$$

where σ_{SB} is the Stefan–Boltzmann constant and R is the stellar radius, also generated by BSE. As for the binaries, also the masses of the 800 single stars were generated using the IMF.

Furthermore, for the 28 blue stragglers plotted in the HRD, the ratio of M_{BS}/M_{TO} was plotted versus initial periastron distance.

8.2.1 Comparison with M67

Finally, the last part of the project involved comparison with observations of the open cluster M67 where a total of 28 blue stragglers have been observed. Hurley et al. (2005) performed a direct N-body model of M67, including cluster dynamics, containing 20 blue stragglers at 4 Gyr, which is the believed age of M67. My aim is to estimate how often BSs are formed from PBE, i.e. in isolation where dynamical interactions with other systems/stars are completely excluded. The expected number of BSs from PBE in M67 was estimated by

$$N_{BS} = N_{\star,tot} \times f_{bin} \times f_{BS/bin} \tag{17}$$

where $N_{\star,tot}$ is the initial number of stars in M67, f_{bin} is the fraction of stars in binary systems and $f_{BS/bin}$ is the fraction of binaries making BSs.

$f_{BS/bin}$ was estimated by evolving 200 000 binaries in BSE, again using the initial binary parameters described in subsection 8.1. M67 is believed to have solar metallicity so $Z = 0.02$ was chosen Tautvaisiene et al. (2000). $f_{BS/bin}$ is then simply the total number of BSs at $t = 4$ Gyr divided by 200 000. f_{bin} was set to 0.44 according to the multiplicity of solar-type stars studied by (Raghavan et al., 2010) who found that 56% of the stars were single while the rest were in binary or higher multiplicity systems.

Estimating $N_{\star,tot}$ however needed some more thinking. Cantat-Gaudin et al. (2018) obtained a list of 1229 clusters including their member-stars, M67 being one of them, using Gaia Data Release 2. 848 members of M67 were recorded, all with apparent Gaia G-band magnitude $m_G < 18$. The star with lowest mass from this sample is therefore the mass corresponding to a star with apparent Gaia G-band magnitude of 18. This mass will from now be denoted as M_{18}. M_{18} was calculated by fitting a function to the relation between apparent magnitude and mass for an isochrone (population of stars with same age but different mass), again using Scipy's cubic interpolation. The isochrone used to calculate M_{18}, from Bressan et al. (2012), had an age of 1 Gyr but we proceed assuming that low mass stars do not evolve significantly. For each star, the absolute Gaia G-band magnitude ($\mathcal{M}_G$) was given and the corresponding apparent G-band magnitude was calculated using

$$m_G = 5log_{10}\left(\frac{d}{10\,\mathrm{pc}}\right) + \mathcal{M}_G \tag{18}$$

where d is the distance in pc. For M67, the distance has been estimated to $d = 857.6$ pc (Cantat-Gaudin et al., 2018). The apparent magnitude was then plotted versus mass (see figure 11) and M_{18} was estimated to be $M_{18} = 0.58\ M_\odot$. The 848 members of M67 then corresponds to the total number of stars today with masses between M_{18} and $M_{TO}(t = 4\,Gyr)$, $N_\star(M > M_{18}, t = 4\,Gyr)$, which can be written in terms of an integral

of the IMF

$$N_\star(M > M_{18}, t = 4\,Gyr) = 848 = C_1 \int_{M_{18}}^{M_{TO}(t=4\,Gyr)} \frac{dN}{dm} dm = C_1 \int_{M_{18}}^{M_{TO}(t=4\,Gyr)} m^{-2.3} dm \tag{19}$$

where C_1 is a constant that depends on e.g. the total mass of the cluster. $N_{\star,tot}$ is then the number of stars in M67 at $t = 0$ with mass $M > M_{18}$ which will be denoted $N_\star(M > M_{18}, t = 0)$ and can also be written in terms of the IMF

$$N_\star(M > M_{18}, t = 0) = C_2 \int_{M_{18}}^{100 M_\odot} m^{-2.3} dm \tag{20}$$

where the upper limit of integration was chosen for consistency with the IMF used when evolving the binaries. If we assume $C_1 = C_2 = C$, we can calculate $N_\star(M > M_{18}, t = 0)$ by taking the ratio of $N_\star(M > M_{18}, t = 4\,Gyr)$ to $N_\star(M > M_{18}, t = 0)$, since we know that $N_\star(M > M_{18}, t = 4\,Gyr)$=848

$$\frac{848}{N_\star(M > M_{18}, t = 0)} = \frac{N_\star(M > M_{18}, t = 4\,Gyr)}{N_\star(M > M_{18}, t = 0)} = \frac{C \int_{M_{18}}^{M_{TO}(t=4\,Gyr)} m^{-2.3} dm}{C \int_{M_{18}}^{100 M_\odot} m^{-2.3} dm}$$

$$= \frac{\left[\frac{-m^{-1.3}}{1.3}\right]_{M_{18}}^{M_{TO}(t=4\,Gyr)}}{\left[\frac{-m^{-1.3}}{1.3}\right]_{M_{18}}^{100 M_\odot}} = \alpha$$

$$\implies N_{\star,tot} = N_\star(M > M_{18}, t = 0) = \frac{848}{\alpha}$$

To correct for the fact that we only consider $M > M_{18}$ I removed all binaries with initial donor mass $M_d < M_{18}$ from the BS population used to calculate $f_{BS/bin}$. Also, the number of input binaries needs to be corrected. The number of input binaries with $M_d > M_{18}$ was calculated by

$$N_{bin}(M_d > M_{18}) = 200000 \times \frac{C \int_{M_{18}}^{100 M_\odot} m^{-2.3} dm}{C \int_{0.5 M_\odot}^{100 M_\odot} m^{-2.3} dm} = 200000 \times \frac{\left[\frac{-m^{-1.3}}{1.3}\right]_{M_{18}}^{100 M_\odot}}{\left[\frac{-m^{-1.3}}{1.3}\right]_{0.5 M_\odot}^{100 M_\odot}}$$

$$= 200000 \times \beta$$

The number of expected BSs from PBE in M67 is thus, rewriting equation 17

$$N_{BS} = \frac{848}{\alpha} \times 0.44 \times \frac{N_{BS}(M_d > M_{18})}{200000 \cdot \beta} = \frac{848}{0.660} \times 0.44 \times \frac{286}{200000 \cdot 0.825} = 0.980 \approx 1$$

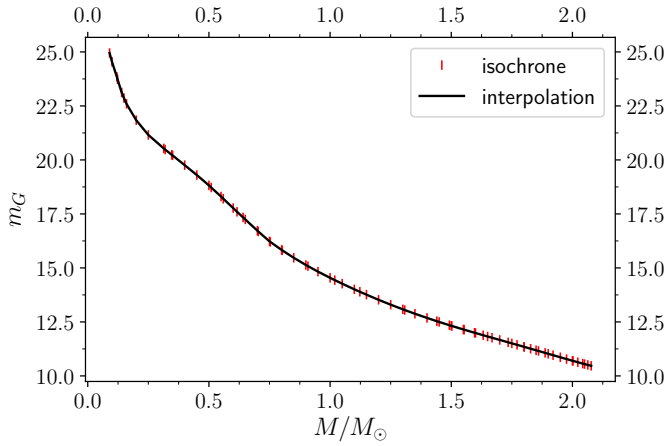

Figure 11: The apparent Gaia G-band magnitude versus stellar mass for an isochrone at t=1 Gyr (Bressan et al., 2012).

8.3 Results

In this subsection I present the results of section 8. In figure 12, the number of BSs formed per binary versus time is plotted, for the three different metallicities. The error-bars corresponds to $\sqrt{N_{BS(t)}}$ where $N_{BS}(t)$ is the number of BSs at time t. Figure 13 and 14 show the fraction of BSs formed by close and wide binaries, respectively.

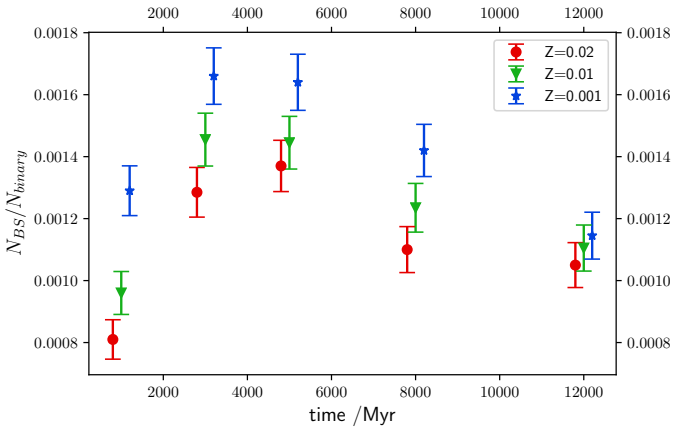

Figure 12: The number of blue stragglers formed per binary versus time at t=1,3,5,8 and 12 Gyr. Note that the data points for $Z = 0.02$ (red) and $Z = 0.001$ (blue) are shifted slightly in the plot to make the results clearer.

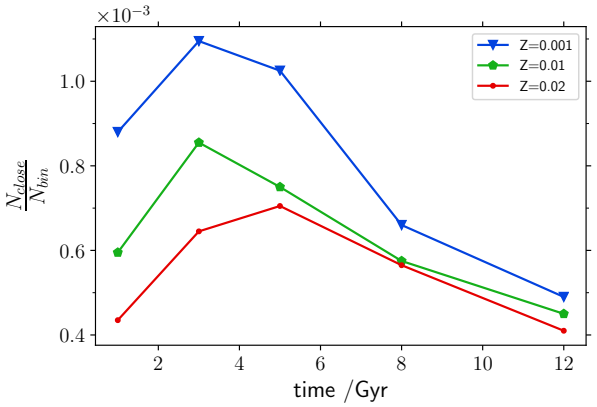

Figure 13: The number of blue stragglers originating from close binaries per binary, versus time.

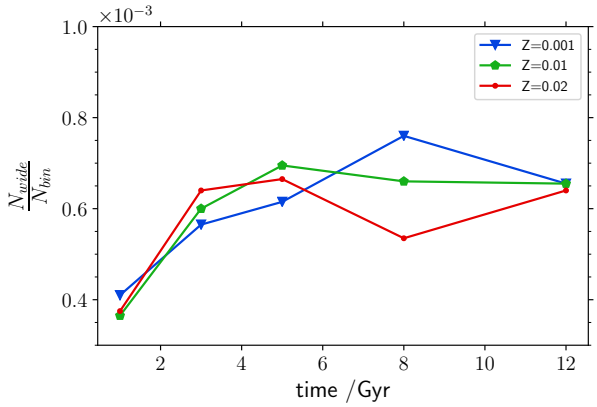

Figure 14: The number of blue stragglers originating from wide binaries per binary, versus time.

In figure 15 the BS populations obtained when evolving 200 000 binaries up to $t = 1, 5$ and 12 Gyr for $Z = 0.02$ are presented. In particular, the plot shows the initial periastron distance of their parent binary versus the initial mass of the accretor. The vertical lines from left to right represents $M_{TO}(t, Z = 0.02)$ at $t = 1, 5$ and 12 Gyr, respectively.

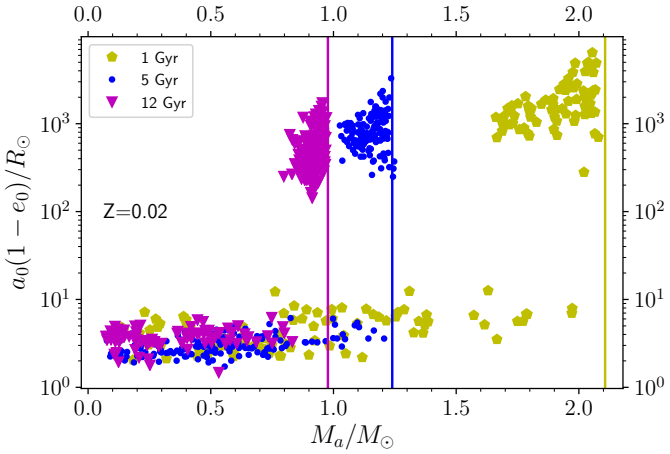

Figure 15: BS populations from evolving 200 000 binaries up to 1 (magenta), 5 (blue) and 12 (yellow) Gyr. Y-values are the initial periastron distance of the parent binary while the x-values are the initial mass of the accretor. The vertical lines in magenta, blue and yellow represents $M_{TO}(t = 12$ Gyr), $M_{TO}(t = 5$ Gyr) and $M_{TO}(t = 1$ Gyr), respectively.

Figure 16 is a HRD including 800 single stars evolved up to 4 Gyr at Z=0.02. The plot also includes 28 BSs, corresponding to the number observed in M67. Further, the ratio of $M_{BS}/M_{TO}(t = 4\,\text{Gyr})$ versus $a_0(1 - e_0)$ of the 28 BSs in figure 16 is plotted in figure 17.

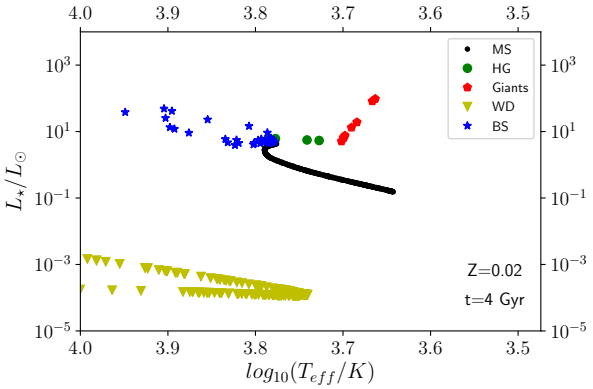

Figure 16: HRD of 800 single stars and 28 BSs.

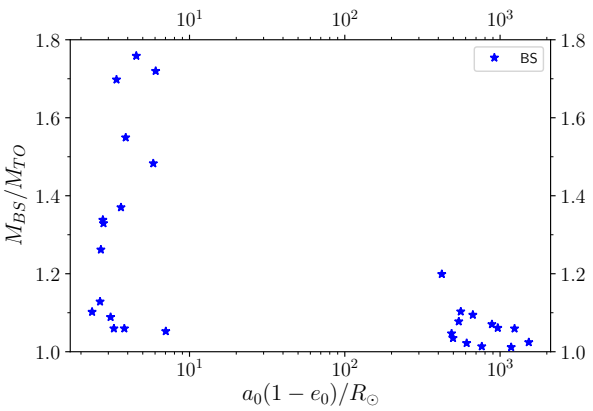

Figure 17: The ratio of BS mass to TO mass at 4 Gyr versus initial periastron distance of the BSs in figure 16.

8.4 Analysis

The reason why considering the distance at periastron (when defining close and wide binaries) for this part instead of the semi major axis as in section 7 was because it turned out that highly eccentric binaries, with e_0 close to one, formed BSs through similar processes as circular binaries with small a_0. Although the initial semi major axis of the highly eccentric binary was large, $a_0(1 - e_0)$ could be small enough for tidal forces to completely circularize the orbit when the two stars met at periastron. For some cases the two stars merged at periastron while for other cases the circularization caused the semi major axis to decrease greatly. We can therefore conclude that it is the initial distance at periastron that will determine the formation pathway of BSs, rather than just a_0.

BSs are formed at any time between 1-12 Gyr, but at different rates. The number of BSs per evolved binary peaks at around 3-5 Gyr, for all three metallicities. The dominant process resulting in the formation of a BS also depends on time. From figure 13 and 14 we see that at 1,3 and 5 Gyr, the BS population is dominated by BSs formed by close binaries. As time increases, the fraction of BSs formed by wide binaries increases, and dominates the population at 12 Gyr. This is probably because t_{BEG}^{BS} is lower for close binaries, since they become BSs directly upon coalescence or large-scale mass transfer. The number of wide binaries making BSs first increases between 1 and 3 Gyr, then stays roughly constant at 5,8 and 12 Gyr.

Furthermore, there is a significant difference between different metallicities, in terms of number of BSs per binary. As seen in figure 12, BSs are formed more frequently at lower metallicities, especially early in the evolution. This is a consequence of the metallicity dependence on the number of BSs from close binaries, as seen in figure 13. This could

potentially be explained by the relation between the metallicity and MS lifetime . Increasing the metallicity typically increases the opacity in the surface regions, at least for solar like stars for which the dominant source of opacity is H^- bound-bound and bound-free transitions. As described in section 4, the luminosity is inversely proportional to the opacity and the MS lifetime is inversely proportional to the luminosity. Thus, metal-poor solar-like stars have shorter lifetime than metal-rich ones. t^{BS}_{BEG} is therefore lower for metal-poor binaries, for a fixed accretor and donor mass. Another explanation for BSs to form more frequently at lower Z might be that mass transfer for close binaries is stable for a larger range of a_0, as can be seen in figure 18 and compared with figure 3. In particular, the range of a_0 for RLOF when the donor is crossing the HG is larger, which again is the region where t^{BS}_{BEG} and t^{BS}_{END} is roughly constant in figure 18. This is because the maximum stellar radius in the HG is larger for stars with Z=0.001 than stars with Z=0.02, since metal-poor stars are more luminous but enters the RGB at a similar T_{eff} as metal-rich stars. Hence, according to equation 16, metal-poor stars need to grow larger in the HG. RLOF when the donor is in the HG can therefore occur at larger separation for metal-poor stars.

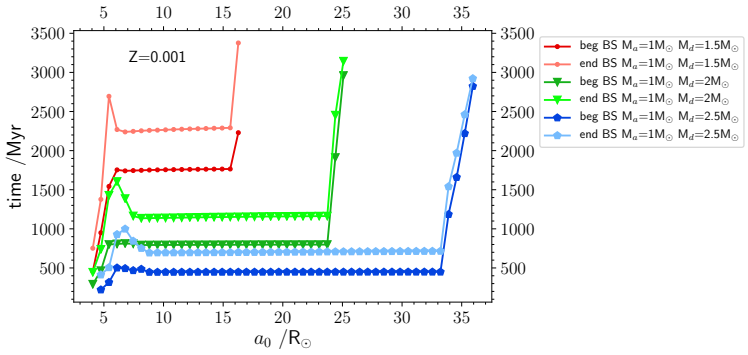

Figure 18: t^{BS}_{BEG} and t^{BS}_{END} versus a_0 for close binaries at Z=0.001.

The frequency of BSs formed by wide binaries however is independent or less dependent on the metallicity. Wind accretion, which is the dominant formation pathway for BSs formed by wide binaries, is therefore less sensitive to Z. This is because giant structures and thus winds are similar for metal-poor and metal-rich stars. However, others have shown that radiation driven stellar wind for massive O-stars are stronger at higher metallicities, e.g. Kudritzki et al. (1989). On the other hand, O-stars are too massive and short-lived to be of any importance for BSs.

The BSs early in the evolution are typically formed by more massive accretor stars as seen in figure 15 which simply is a consequence of the decrease in TO mass with time. Furthermore, only initial accretor masses below $\sim 2M_\odot$ form blue stragglers after 1 Gy. For wide binaries, the initial accretor mass is around the TO mass, while for close binaries, the range of initial accretor masses is larger. This is because much less mass is

transferred in wide binaries, the accretor therefore needs to have an initial mass around the TO in order to make it a BS. Closer binaries transfer much more mass. The initial mass of the accretor can thus be much lower than the TO and still produce a BS.

The results in figure 16 and 17 show that the most luminous blue stragglers are produced by close binaries. This is again a consequence of more mass being transferred in close binaries. These will thus more easily be detected since they are more prominent in the HRD.

Finally, for the comparison with the BSs in M67. The number of BSs from PBE in M67 was estimated to be roughly 1, which is much less than the 28 observed (Hurley et al., 2005). There are many reasons why the number turned out to be lower than expected. Firstly, lower mass objects are more likely to be ejected from the cluster, meaning that f_{bin} might actually be larger than 0.44. Secondly, there is a large uncertainty of the initial number of stars in M67. However, as many as 29 times more stars would have been needed to reproduce 28 BSs from PBE, using the estimated value of $f_{BS/bin}$ and $f_{bin} = 0.44$. The results therefore indicate that PBE alone can't explain the total number of BSs in M67. Lastly, if a larger portion of the binaries were in short period orbits, then the fraction of $f_{BS/bin}$ would increase significantly. As mentioned in subsection 8.1, I used a log Gaussian distribution of periods with peak at $log(P/days) = 5.03$ and standard deviation $\sigma_{logP} = 2.28$ found by Raghavan et al. (2010). However, others have suggested, based on observations, a flat distribution of $log(a_0)$, e.g. Abt (1983). Hurley et al. (2001) studied what choice of initial binary parameters would maximize the BS formation rate when evolving binary populations, also using the BSE code by Hurley et al. (2002). They found, by using a flat $log(a_0)$ distribution, that PBE alone could explain the total number of BSs in M67 (assuming no BSs were ejected over its lifetime), without the need of cluster dynamics. On the other hand, they also found that their BS population was very different from observations. For instance, of the total 28 BSs observed in M67, only 25% are in binary systems. They could therefore conclude that cluster dynamics must have an essential role in altering the nature of the population, but perhaps not to explain the creation of them.

9 Summary

A blue straggler is a main sequence star more luminous and hotter than the turnoff, which makes it appear younger than the rest of the stars within the population. Blue stragglers are believed to form by mass transfer in binary systems or by stellar collisions. Here, I have only considered blue stragglers formed from primordial binary evolution, excluding any dynamical effects.

To fully understand the nature and properties of blue stragglers from PBE, a substantial amount of stellar evolution, in particular binary evolution, need to be incorporated. Fur-

thermore, concepts like Roche lobe, RLOF, circularization and stability of mass transfer are essential to explain their existence. With the help of the rapid BSE code by (Hurley et al., 2002), it is possible study them in great detail both individually and by reproducing BS populations. During this project, I have shown that the initial distance at periastron determines the formation pathway of the BSs. If we also include the masses of the two components and their metallicity, it is possible to deduce whether the mass transfer will be stable or not, and its rate. There exists two regions of $a_0(1 - e_0)$, corresponding to different stellar phases of the donor when RLOF occurs, for which the mass transfer is stable. Close binaries have stable mass transfer when the donor is on the MS and in the HG while wide binaries have stable mass transfer once $q = \frac{M_d}{M_a} < q_{crit}$, which typically is fulfilled when the donor is on the AGB. For that reason, RLOF and mass transfer on the RGB is almost exclusively unstable.

I have also shown, in figure 15, that in stellar population older than 1 Gyr, only stars with masses below $\sim 2\ M_\odot$ become BSs. The stars that form BSs by wind accretion or when the donor is on the AGB have initial masses around the TO, while close binaries form BSs for a larger range of accretor masses. The most massive and luminous BSs, compared to the TO, originates from large-scale mass transfer within close binaries, or from the coalescence of the two components. BSs formed by wind accretion or RLOF on the AGB are therefore more difficult to detect.

BSs form at any time during the evolution, but their relative frequency peaks at around 3-5 Gyr. For young binary populations, the fraction of BSs formed by close binaries dominates, but eventually decreases with time. At 12 Gyr, the BSs from wide binaries dominate the population. Furthermore, the frequency of BSs is higher at lower metallicities. This could be explained by the larger range of initial periastron distances allowing for stable mass transfer at lower metallicities.

In the end, I compared the derived frequency of BSs from PBE to the open cluster M67, containing 28 BSs. The estimated frequency was too low to explain the number observed in M67. This could be a consequence of the uncertainty in e.g. binary fraction, initial number of stars in the cluster, the initial binary parameters or that cluster dynamics needs to be included to explain the existence of a large fraction of them.

Improving the understanding of blue stragglers can be useful when studying cluster environments, binary evolution or when determine the age of stellar populations. To make more accurate models of stellar populations in globular or open clusters it is necessary to improve the understanding of their initial conditions, the distribution of orbital parameters within these systems, the IMF and its dynamical evolution, which hopefully can be achieved by further observations and studies.

References

Abt, H. A.: 1983, *ARA&A* **21**, 343

Beccari, G. and Carraro, G.: 2015, in H. M. J. Boffin, G. Carraro, and G. Beccari (eds.), *Astrophysics and Space Science Library*, Vol. 413 of *Astrophysics and Space Science Library*, p. 1

Boffin, H. M. J.: 2015, in H. M. J. Boffin, G. Carraro, and G. Beccari (eds.), *Astrophysics and Space Science Library*, Vol. 413 of *Astrophysics and Space Science Library*, p. 153

Boffin, H. M. J., Carraro, G., and Beccari: 2015, *Ecology of Blue Straggler Stars*, Springer-Verlag Berlin Heidelberg

Bondi, H. and Hoyle, F.: 1944, *MNRAS* **104**, 273

Bressan, A., Marigo, P., Girardi, L., Salasnich, B., Dal Cero, C., Rubele, S., and Nanni, A.: 2012, *MNRAS* **427(1)**, 127

Camargo, D. and Minniti, D.: 2019, *MNRAS* **484(1)**, L90

Cantat-Gaudin, T., Jordi, C., Vallenari, A., Bragaglia, A., Balaguer-Núñez, L., Soubiran, C., Bossini, D., Moitinho, A., Castro-Ginard, A., Krone-Martins, A., Casamiquela, L., Sordo, R., and Carrera, R.: 2018, *A&A* **618**, A93

Clarkson, W. I., Sahu, K. C., Anderson, J., Rich, R. M., Smith, T. E., Brown, T. M., Bond, H. E., Livio, M., Minniti, D., Renzini, A., and Zoccali, M.: 2011, *ApJ* **735(1)**, 37

Eggleton, P. P.: 1983, *ApJ* **268**, 368

Eldridge, J. J. and Tout, C. A.: 2019, *The Structure and Evolution of Stars*, World Scientific Publishing Europe Ltd, London, UK

Gray, D. F.: 2008, *The Observation and Analysis of Stellar Photospheres*, Cambridge University Press, New York

Hurley, J. R., Pols, O. R., Aarseth, S. J., and Tout, C. A.: 2005, *MNRAS* **363(1)**, 293

Hurley, J. R., Pols, O. R., and Tout, C. A.: 2000, *MNRAS* **315(3)**, 543

Hurley, J. R., Tout, C. A., Aarseth, S. J., and Pols, O. R.: 2001, *MNRAS* **323(3)**, 630

Hurley, J. R., Tout, C. A., and Pols, O. R.: 2002, *MNRAS* **329(4)**, 897

Ivanova, N.: 2015, in H. M. J. Boffin, G. Carraro, and G. Beccari (eds.), *Astrophysics and Space Science Library*, Vol. 413 of *Astrophysics and Space Science Library*, p. 179

Jofré, P., Jorissen, A., Van Eck, S., Izzard, R. G., Masseron, T., Hawkins, K., Gilmore, G., Paladini, C., Escorza, A., Blanco-Cuaresma, S., and Manick, R.: 2016, *A&A* **595**, A60

Kroupa, P.: 2001, *MNRAS* **322(2)**, 231

Kudritzki, R. P., Pauldrach, A., Puls, J., and Abbott, D. C.: 1989, *A&A* **219**, 205

Lagarde, N., Decressin, T., Charbonnel, C., Eggenberger, P., Ekström, S., and Palacios, A.: 2012, *A&A* **543**, A108

Martig, M., Rix, H.-W., Silva Aguirre, V., Hekker, S., Mosser, B., Elsworth, Y., Bovy, J., Stello, D., Anders, F., García, R. A., Tayar, J., Rodrigues, T. S., Basu, S., Carrera, R., Ceillier, T., Chaplin, W. J., Chiappini, C., Frinchaboy, P. M., García-Hernández, D. A., Hearty, F. R., Holtzman, J., Johnson, J. A., Majewski, S. R., Mathur, S., Mészáros, S., Miglio, A., Nidever, D., Pan, K., Pinsonneault, M., Schiavon, R. P., Schneider, D. P., Serenelli, A., Shetrone, M., and Zamora, O.: 2015, *MNRAS* **451(2)**, 2230

Mateo, M., Harris, H. C., Nemec, J., and Olszewski, E. W.: 1990, *AJ* **100**, 469

Mateo, M., Nemec, J., Irwin, M., and McMahon, R.: 1991, *AJ* **101**, 892

Moe, M. and Di Stefano, R.: 2017, **230(2)**, 15

Moe, M., Kratter, K. M., and Badenes, C.: 2019, *ApJ* **875(1)**, 61

Mowlavi, N., Meynet, G., Maeder, A., Schaerer, D., and Charbonnel, C.: 1998, *A&A* **335**, 573

Paczyński, B.: 1971, *ARA&A* **9**, 183

Preston, G. W. and Sneden, C.: 2000, *AJ* **120(2)**, 1014

Raghavan, D., McAlister, H. A., Henry, T. J., Latham, D. W., Marcy, G. W., Mason, B. D., Gies, D. R., White, R. J., and ten Brummelaar, T. A.: 2010, **190(1)**, 1

Sandage, A. R.: 1953, *AJ* **58**, 61

Tautvaisiene, G., Edvardsson, B., Tuominen, I., and Ilyin, I.: 2000, *VizieR Online Data Catalog* pp J/A+A/360/499

Tout, C. A., Aarseth, S. J., Pols, O. R., and Eggleton, P. P.: 1997, *MNRAS* **291(4)**, 732

Wyse, R. F. G., Moe, M., and Kratter, K. M.: 2020, *MNRAS* **493(4)**, 6109

Zhao, Z., Okamoto, S., Arimoto, N., Aoki, W., and Kodama, T.: 2012, in W. Aoki, M. Ishigaki, T. Suda, T. Tsujimoto, and N. Arimoto (eds.), *Galactic Archaeology: Near-Field Cosmology and the Formation of the Milky Way*, Vol. 458 of *Astronomical Society of the Pacific Conference Series*, p. 349